





Metal-insulator transition in $\text{Ba}_{3-x}\text{Sr}_x\text{Nb}_5\text{O}_{15}$ Yuhki Kondoh,¹ Ryosuke Takei,¹ Tetsuji Okuda,² Kazunori Ueno ,³ Yumiko Katayama ,³ Takuo Saiki,¹ Wataru Sekino,¹ Tomomasa Kajita ,¹ and Takuro Katsufuji ^{1,4}¹*Department of Physics, Waseda University, Tokyo 169-8555, Japan*²*Graduate School of Science and Engineering, Kagoshima University, Kagoshima 890-0065, Japan*³*Department of Basic Science, University of Tokyo, Meguro, Tokyo 153-8902, Japan*⁴*Kagami Memorial Research Institute for Materials Science and Technology, Waseda University, Tokyo 169-0051, Japan*

(Received 7 June 2021; revised 16 August 2021; accepted 8 September 2021; published 20 September 2021)

We investigated single crystals of $\text{Ba}_{3-x}\text{Sr}_x\text{Nb}_5\text{O}_{15}$ with a tetragonal tungsten bronze (TTB) structure, which exhibits a metal-insulator transition with x . We found that there is a one-dimensional anisotropy with a higher dc conductivity along the c axis in the metallic phase, but it disappears in the insulating phase. The optical conductivity spectra of the metallic samples show similar anisotropy to the dc conductivity, but the anisotropy persists even in the insulating phase. These experimental results, together with the result of magnetic susceptibility, indicate that the disorder caused by the Sr ions loosely bound to the surrounding oxygen ions plays an important role in the metal-insulator transition.

DOI: [10.1103/PhysRevB.104.125128](https://doi.org/10.1103/PhysRevB.104.125128)**I. INTRODUCTION**

Metal-insulator transitions are phenomena in which electrical resistivity changes by many orders of magnitude with temperature, pressure, or the composition of the compounds [1]. Regarding the metal-insulator transitions caused by a compositional change, the origins can be categorized into two groups: (a) those caused by changes in the Fermi level, i.e., by carrier doping, and (b) those caused by changes without carrier doping. The former includes a phase transition from a band insulator to a doped conductor and that from a Mott insulator, where an integer number of electrons at each site are localized owing to the on-site Coulomb repulsion, to a metal with carrier doping (a Mott transition) [2]. The latter includes a different type of Mott transition, i.e., a transition from a Mott insulator to a metal with a change in bandwidth, and a transition from a band insulator to a semimetal with a shift of the valence and conduction bands. Another metal-insulator transition categorized into (b) is a transition from a metal to an Anderson insulator (Anderson localization) caused by disorders.

$\text{Ba}_{3-x}\text{Sr}_x\text{Nb}_5\text{O}_{15}$ ($0 \leq x \leq 3$) [3–7] is a series of compounds with a tetragonal tungsten bronze (TTB) structure (the space group P_4mbm). This crystal structure can be regarded as a modified perovskite structure, as illustrated in Fig. 1. Each Nb ion is surrounded by six oxygen ions in an octahedral configuration, and these NbO_6 octahedra (shown by squares in Fig. 1) share corners with each other. Compared with the perovskite structure, additional NbO_6 octahedra are inserted in the TTB structure; thus, the NbO_6 octahedra are connected in a zigzag manner along the ab plane of the tetragonal structure, whereas the connection remains straight (the Nb-O-Nb bond angle is 180°) along the c axis. The formal valence of Nb is $4.8+$, meaning that there are 0.2 electrons on average per Nb,

and this does not change with x in this series of compounds. Nevertheless, they exhibit a metal-insulator transition with x ; it is metallic when $x = 0$, but it is insulating when $x = 3$, although its mechanism remains unclarified.

Another unclarified issue on this series of compounds is the anisotropy of the electronic structure and the transport properties. There are various compounds with the TTB structure and hexagonal tungsten bronze (HTB) structure, which is also composed of corner-shared AO_6 octahedra, and some of them exhibit the superconducting property at low temperatures [6,8–11]. However, little is known about the anisotropy of compounds with these crystal structures, except for a paper on Na_xWO_3 [12]. In relation to the issue of anisotropy, $\text{Ba}_{3-x}\text{Sr}_x\text{Nb}_5\text{O}_{15}$ in polycrystalline forms exhibit a large Seebeck coefficient, particularly at high temperatures ($S \sim 100 \mu\text{V}/\text{K}$ near 1000 K) [6], and it is interesting to see if the thermoelectric property can be enhanced by using a particular orientation of a single crystal.

In this paper, we grew single crystals of $\text{Ba}_{3-x}\text{Sr}_x\text{Nb}_5\text{O}_{15}$ and investigated their various properties to clarify the origin of the metal-insulator transition and the anisotropy of the electronic structure.

II. EXPERIMENT AND BAND CALCULATION

Single crystals of $\text{Ba}_{3-x}\text{Sr}_x\text{Nb}_5\text{O}_{15}$ ($0 \leq x \leq 2$) were grown by the floating-zone technique. The starting materials were BaCO_3 , SrCO_3 , and Nb_2O_5 , and their stoichiometric amounts were mixed and pressed into a rod, and the rod was sintered at 1300°C for 12 hours in a 7% H_2/Ar gas. The sintered rod was melted in a floating-zone furnace in a 7% H_2/Ar gas, and single crystals were grown at a feed speed of 8 mm/h. The grown crystals were checked by x-ray powder diffraction measurement. We found that the single crystals for

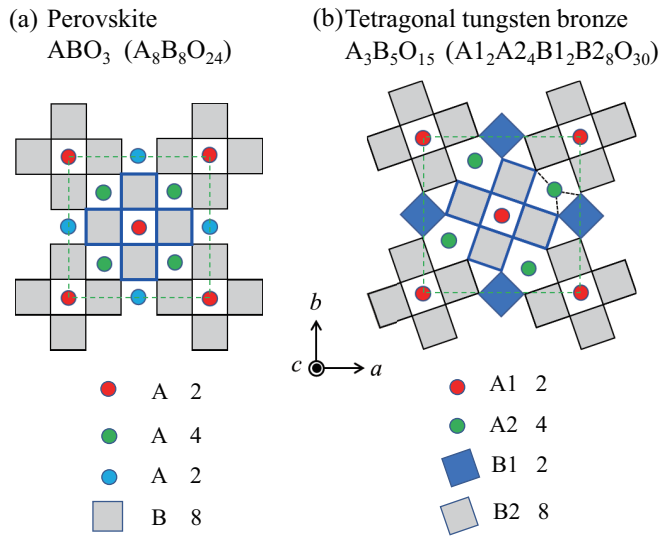


FIG. 1. Crystal structures of (a) perovskite structure (ABO_3) and (b) tetragonal tungsten bronze (TTB) structure ($A_3B_5O_{15}$). Each square corresponds to a BO_6 octahedron viewed from the vertical direction and each circle corresponds to an A ion. The B ions exist at the centers of the squares, and the oxygen ions exist at the corners of the squares. Note that the A ion is shifted from the B ion by half the height of the BO_6 octahedron perpendicular to the plane. In (b), blue squares are newly inserted whereas the blue circles in (a) disappear. The three dotted lines from the A2 ion indicate the six oxygen ions (three above and three below are overlapped in the figure) nearest to it.

$x \geq 2.5$ cannot be grown but the A-site-deficient perovskite appears when using this method, although polycrystalline samples with the TTB structure in this compositional range can be easily synthesized.

The orientation of the grown crystals was determined by the Laue method. The offstoichiometry of the crystals was determined by induction-coupled plasma (ICP) analysis and thermogravimetric analysis (TGA). We found that the composition of our single crystals is $Ba_3Nb_5O_{15.08}$ ($n = 0.17$, where n corresponds to the nominal number of d electrons per Nb) for $x = 0$, $Ba_{1.5}Sr_{1.57}Nb_{4.96}O_{14.85}$ ($n = 0.25$) for $x = 1.5$, and $Ba_1Sr_{1.94}Nb_{4.82}O_{14.57}$ ($n = 0.17$) for $x = 2.0$. This confirms that the change in the nominal number of d electrons in Nb is not the origin of the metal-insulator transition.

Resistivity and Hall measurements were performed using silver paste cured at room temperature as electrodes. For the Hall measurement, the magnetic field was applied between -7 and 7 T perpendicular to the current direction. Magnetic susceptibility was measured by a SQUID magnetometer. The Seebeck coefficient and resistivity at high temperatures were simultaneously measured in helium gas at negative pressure by a four-probe method, where an R-type thermocouple was used to measure both the temperature difference and thermoelectromotive force. The polarized optical reflectivity was measured on the polished ac plane of the single crystals using a grating spectrometer between 0.7 and 5 eV and an FTIR spectrometer between 0.1 and 0.8 eV at room temperature.

First-principles calculations were performed on the basis of the plane wave density functional theory using the Quantum

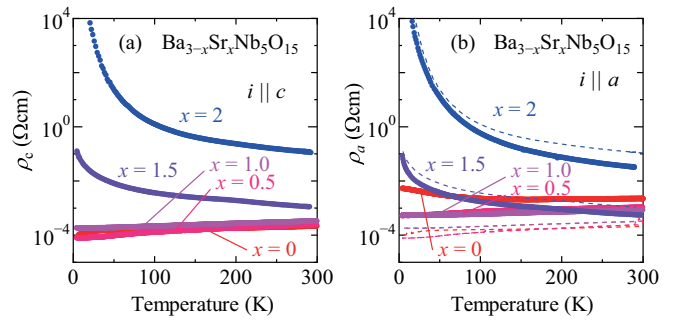


FIG. 2. Temperature dependence of resistivity for $Ba_{3-x}Sr_xNb_5O_{15}$ along the (a) c and (b) a axes. The dashed lines in (b) refer to the resistivity along the c axis shown in (a).

Espresso (QE) simulation package [13]. We employed the local density approximation without on-site Coulomb repulsion (U). A tetragonal primitive cell consisting of $Ba_6Nb_{10}O_{30}$ was used. The atom positions and lattice parameters were taken from Ref. [6]. The atoms were represented by norm-conserving pseudopotentials from the QE library with the fhi98PP pseudopotential program [14]. The cutoff kinetic energy for charge density and potential calculations was set to 350 eV. The transport properties were calculated from a band structure with a $20 \times 20 \times 20$ k -point mesh using the BoltzTraP program [15].

III. RESULTS

Figure 2 shows the temperature (T) dependence of the resistivity along the c axis (ρ_c) and a axis (ρ_a). The behavior of resistivity changes from being metallic ($d\rho/dT > 0$, $x \leq 1$) to insulating ($d\rho/dT < 0$, $x \geq 1.5$) with increasing x , as similarly observed in polycrystalline samples previously reported [6]. Furthermore, there is anisotropy of approximately one order of magnitude ($\rho_c < \rho_a$) for the metallic samples ($x \leq 1$). This is more clearly seen in Fig. 3, where ρ_c and ρ_a for two different samples with $x = 0$ in a linear scale are shown as a function of T . As can be seen, ρ_c keeps decreasing whereas ρ_a increases below 120 K with decreasing T for the

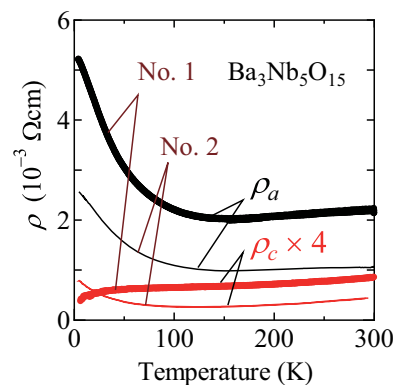


FIG. 3. Temperature dependence of resistivity for two different samples, No. 1 (thick lines) and No. 2 (thin lines), of $Ba_3Nb_5O_{15}$ along the a axis (ρ_a) and c axis (ρ_c). The data of ρ_c is multiplied by four for clarity.

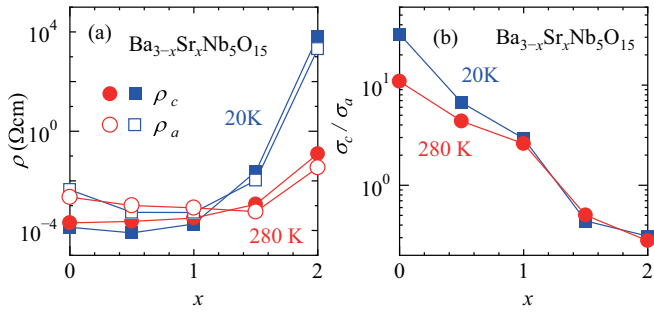


FIG. 4. (a) Resistivity of $\text{Ba}_{3-x}\text{Sr}_x\text{Nb}_5\text{O}_{15}$ at 280 K (red circles) and 20 K (blue squares) along the c axis (ρ_c , closed symbols) and a axis (ρ_a , open symbols) as a function of x . (b) Anisotropy of resistivity, σ_c/σ_a , at 280 K (red circles) and 20 K (blue squares) as a function of x .

No. 1 sample (as shown in Fig. 2), but an upturn is observed also in the T dependence of ρ_c for the No. 2 sample. We speculate that the upturn in ρ_c for the No. 2 sample, which has a lower resistivity than the No. 1 sample, arises from the misalignment of the crystal, resulting in the mixture of the ρ_a component with a larger absolute value in the measurement of ρ_c . Such anisotropy in the resistivity can be qualitatively explained by their zigzag Nb-O-Nb bonds along the ab plane (Fig. 1) and the straight Nb-O-Nb bonds along the c axis.

Figure 4(a) shows the x dependence of ρ_c (closed symbols) and ρ_a (open symbols) at 280 K (circles) and 20 K (squares). The magnitude of resistivity increases for $x > 1$, particularly at 20 K. Here, we define the anisotropy of conductivity as $\sigma_c/\sigma_a = \rho_a/\rho_c$, where $\sigma_i = 1/\rho_i$ is the conductivity in the i direction ($i = a, c$), and we plot it at 280 K and 20 K in a log scale as a function of x in Fig. 4(b). σ_c/σ_a is largest for $x = 0$, which is on the order of 10, but it gradually decreases with increasing x and becomes smaller than unity for $x > 1$. These results are summarized as follows: for $x < 1$, this series of compounds are metallic with the anisotropy of $\sigma_c > \sigma_a$, but they become insulating for $x > 1$ with least anisotropy.

To investigate the anisotropy of this series of compounds in more detail, we measured the polarized optical reflectivity spectra for the single crystals. Figure 5 shows the reflectivity spectra with $E \parallel c$ [$R_c(\omega)$] and $E \parallel a$ [$R_a(\omega)$] for various

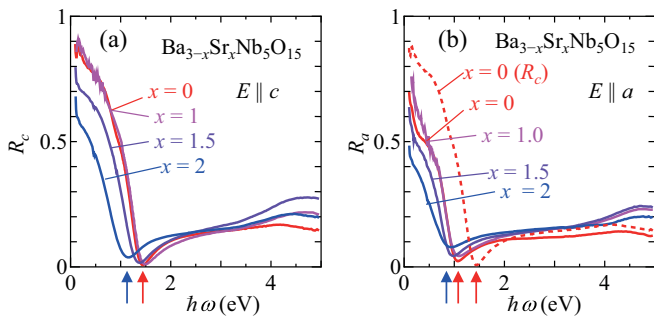


FIG. 5. Reflectivity spectra of $\text{Ba}_{3-x}\text{Sr}_x\text{Nb}_5\text{O}_{15}$ at room temperature with the polarization along (a) the c axis (R_c) and (b) a axis (R_a). The dashed line in (b) is R_c with $x = 0$ shown in (a). The arrows show the position of the plasma edge $\hbar\omega_p$ for $x = 0$ and 2.

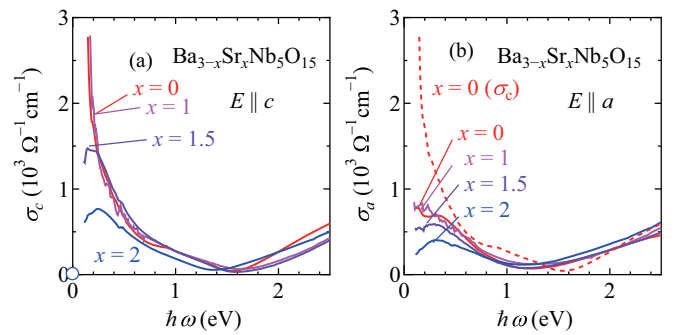


FIG. 6. Optical conductivity spectra of $\text{Ba}_{3-x}\text{Sr}_x\text{Nb}_5\text{O}_{15}$ at room temperature along (a) the c axis (σ_c) and (b) a axis (σ_a). The dashed line in (b) is σ_c with $x = 0$ shown in (a). The open circle in (a) corresponds to the dc conductivity along the c axis for $x = 2$.

values of x at room temperature. A Drude-like spectrum, i.e., large values at low $\hbar\omega$, a sharp decrease and an edge (a plasma edge, whose position is referred to as $\hbar\omega_p$, as indicated by arrows in Fig. 5), and a relatively flat $\hbar\omega$ dependence at higher than the plasma edge, is observed both for $R_c(\omega)$ and $R_a(\omega)$ for all x . However, $\hbar\omega_p$ decreases with increasing x both for $R_c(\omega)$ and $R_a(\omega)$ [Figs. 5(a) and 5(b)], and $\hbar\omega_p$ is larger for $R_c(\omega)$ than for $R_a(\omega)$ with the same x [Fig. 5(b)].

Figure 6 shows the optical conductivity spectra derived from the $R(\omega)$ spectra shown in Fig. 5 by the Kramers-Kronig transformation. The open circle in Fig. 6(a) corresponds to the dc conductivity for $x = 2$. In this figure, a Drude spectrum of the optical conductivity, i.e., a Lorentz function centered at $\hbar\omega = 0$, is observed for $E \parallel c$ [$\sigma_c(\omega)$] with $x = 0$ and 1, but it changes to a spectrum with a peak at finite $\hbar\omega$ for $x \geq 1.5$. The optical conductivity spectra for $E \parallel a$ [$\sigma_a(\omega)$] behaves similarly to $\sigma_c(\omega)$ with x , but the spectral weight for $\sigma_a(\omega)$ below 1.4 eV is smaller than that for $\sigma_c(\omega)$ [Fig. 6(b)]. Such anisotropy, which is characteristic of materials with a one dimensional conduction, has been observed in various transition-metal oxides [16–19]. We estimated the spectral weight by integrating the optical conductivity below 1.4 eV and plot it as a function of x in Fig. 7. As can be seen, the spectral weight for $\sigma_c(\omega)$ (W_c) is approximately twice that for $\sigma_a(\omega)$ (W_a) at $x = 0$, and both decrease with increasing

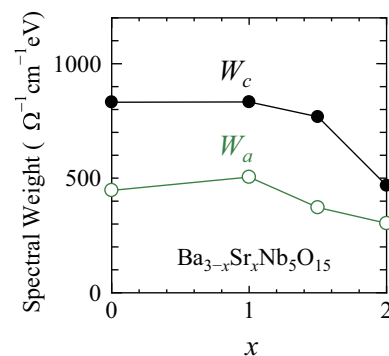


FIG. 7. Spectral weight of optical conductivity below 1.4 eV as a function of x for σ_c (W_c , closed circles) and σ_a (W_a , open circles) of $\text{Ba}_{3-x}\text{Sr}_x\text{Nb}_5\text{O}_{15}$.

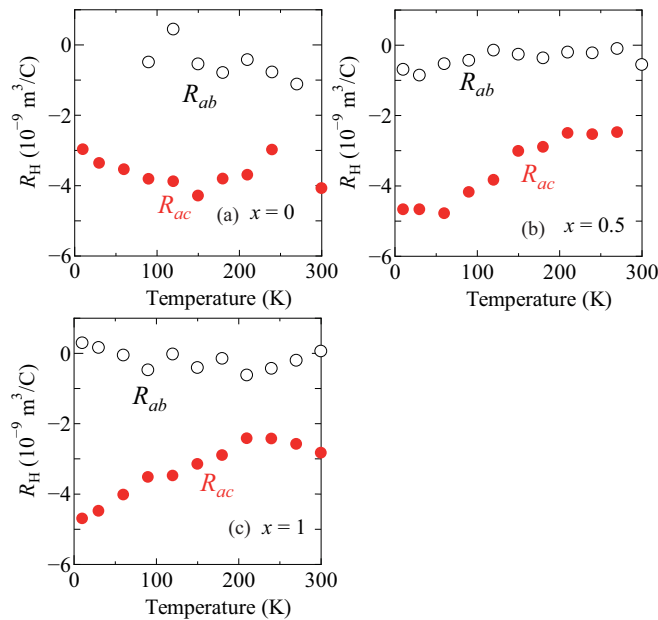


FIG. 8. Hall coefficient along the ac plane (R_{ac} , closed circles) and ab plane (R_{ab} , open circles) as a function of temperature for $\text{Ba}_{3-x}\text{Sr}_x\text{Nb}_5\text{O}_{15}$ with (a) $x = 0$, (b) $x = 0.5$, and (c) $x = 1.0$.

x , although W_c decreases more significantly, and as a result, the anisotropy in the spectral weight (W_c/W_a) decreases with increasing x .

Here, we point out the qualitative similarity as well as a quantitative discrepancy between the dc conductivity [Fig. 4(b)] and the spectral weight of the optical conductivity (Fig. 7). Qualitatively, both the spectral weight and dc conductivity decrease with increasing x , and the anisotropy becomes smaller with increasing x for both quantities. However, the dc conductivity at room temperature is suppressed by two or three orders of magnitude from $x = 0$ to $x = 2$, whereas the spectral weight decreases only by a factor of two with x . The anisotropy of the dc conductivity for $x = 0$ is $\sigma_c/\sigma_a \sim 10$, but that of the spectral weight for $x = 0$ is $W_c/W_a \sim 2$. On the other hand, σ_c/σ_a is almost unity for $x \geq 1.5$ in the insulating phase, but W_c/W_a is clearly larger than unity for $x \geq 1.5$. Such discrepancies suggest that the metal-insulator transition in this series of compounds is dominated mainly by an energy scale of smaller than 1.4 eV, although the behavior at around 1.4 eV may partially affect the phenomenon.

Figure 8 shows the temperature dependence of the Hall coefficient for $x = 0, 0.5$, and 1. R_{ac} was measured with the current direction $j \parallel c$, the voltage direction $E \parallel a$, and the magnetic-field direction $H \parallel b$, whereas R_{ab} was measured with $j \parallel a$, $E \parallel b$, and $H \parallel c$. As can be seen, R_{ac} is on the order of $\sim -4 \times 10^{-9} \text{ m}^3/\text{C}$, which corresponds to ~ 0.1 electrons per Nb based on the simple free electron model of $R_H = 1/ne$, and it exhibits only a small variation with T or x . On the other hand, R_{ab} is almost zero at all T and x . The anisotropy in the Hall coefficient can be explained by the Fermi surface of one-dimensional metals, as discussed below. The x dependence of the Hall coefficient indicates that the electronic structure of this series of compounds barely

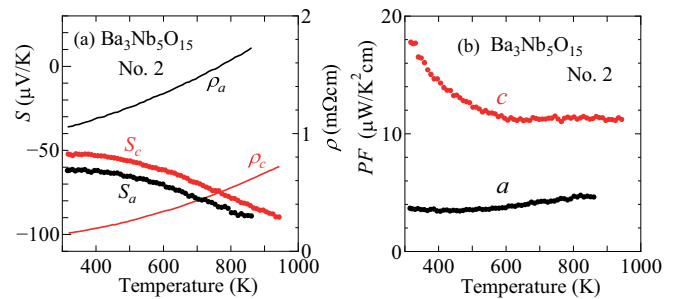


FIG. 9. (a) Seebeck coefficient (thick lines, left axis) and resistivity (thin lines, right axis) for $\text{Ba}_3\text{Nb}_5\text{O}_{15}$ from 300 to 900 K along the c and a axes. (b) Power factor $PF = S^2/\rho$ for $\text{Ba}_3\text{Nb}_5\text{O}_{15}$ along the c and a axes.

changes for $x \leq 1$, even though the metal-insulator transition occurs at around $x \sim 1$.

As discussed in the Introduction, $\text{Ba}_3\text{Nb}_5\text{O}_{15}$ is a good n -type thermoelectric material at high temperatures in a polycrystalline form [6]. We measured the Seebeck coefficient S and the resistivity ρ of our single crystal both along the c and a axes up to 900 K, as shown in Fig. 9. Although there is a factor of 10 anisotropy in ρ , S along the c axis and that along the a axis are nearly the same. As a result, the power factor $PF = S^2/\rho$ along the c axis becomes as high as $\sim 18 \mu\text{W}/\text{K}^2\text{cm}$ at room temperature and $\sim 10 \mu\text{W}/\text{K}^2\text{cm}$ at 900 K, which is several times larger than that along the a axis, and is comparable to that of doped SrTiO_3 [20,21], which is a promising n -type thermoelectric oxide at high temperatures. Note that the Seebeck coefficient is given by $(\pi^2 k_B^2 T / 3q)(\sigma'(E_F)/\sigma(E_F))$, where $\sigma(E)$ is the conductivity when the Fermi level is located at E and $\sigma'(E)$ is its energy derivative. Thus, if all the conduction carriers have the same mass tensor with anisotropy, the anisotropy of the mass tensor does not produce any anisotropy in the Seebeck coefficient since it is canceled when dividing $\sigma'(E_F)$ by $\sigma(E_F)$, whereas the anisotropy in the electrical conductivity is inversely proportional to the anisotropy of the mass tensor. Accordingly, the power factor can be enhanced compared with that of the polycrystalline form by utilizing a specific direction (with a smaller mass tensor) of the single crystal, where a smaller resistivity can be realized without reducing the Seebeck coefficient. This is consistent with the present experimental result shown in Fig. 9. Note that such an absence of the anisotropy in the Seebeck coefficient in spite of a large anisotropy in the resistivity has been observed in some cobaltites [22].

Transport properties were also examined from the calculated band structure. Figure 10 shows the band structure of $\text{Ba}_3\text{Nb}_5\text{O}_{15}$. With the stoichiometric composition, where 0.2 electrons per Nb site exist, there are two bands with smaller dispersion and several bands with larger dispersion along the Γ -Z direction around the Fermi energy. The former two bands have two-dimensional cylindrical Fermi surfaces, whereas the latter bands have one-dimensional sheet-like Fermi surfaces perpendicular to the Z direction, as shown in the upper panels of Fig. 11. With the decreased Fermi energy, however, the two-dimensional cylindrical Fermi surfaces disappear and the one-dimensional sheet-like Fermi surfaces survive, as shown

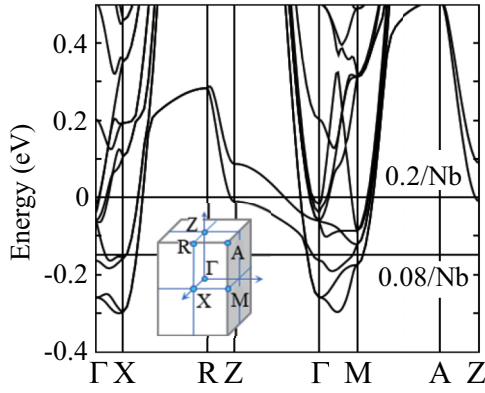


FIG. 10. Band structure of $\text{Ba}_3\text{Nb}_5\text{O}_{15}$. The inset shows the symmetry labels for the primitive tetragonal lattice.

in Fig. 10 and the lower panels of Fig. 11, and they seem to dominate the anisotropy of the transport properties.

To evaluate the anisotropy quantitatively, the transport properties were calculated on the basis of the Boltzmann theory [15]. The electric current j along the α axis ($\alpha = x, y, z$) can be written in terms of the conductivity tensors σ with the

electric field \mathbf{E} and magnetic field \mathbf{B} :

$$j_\alpha = \sum_\beta \sigma_{\alpha\beta} E_\beta + \sum_{\beta,\gamma} \sigma_{\alpha\beta\gamma} E_\beta B_\gamma \quad (1)$$

where E_β and B_γ ($\beta, \gamma = x, y, z$) are the components of \mathbf{E} and \mathbf{B} along the β and γ directions, respectively. The conductivity tensors $\sigma_{\alpha\beta}$ and $\sigma_{\alpha\beta\gamma}$ in Eq. (1) are defined as follows. At the crystal momentum \mathbf{k} with the band index i , the local conductivity tensors can be expressed as

$$\begin{aligned} \sigma_{\alpha\beta}(i, \mathbf{k}) &= e^2 \tau_{i,\mathbf{k}} v_\alpha(i, \mathbf{k}) v_\beta(i, \mathbf{k}), \\ \sigma_{\alpha\beta\gamma}(i, \mathbf{k}) &= \sum_{\mu,\nu} e^3 \tau_{i,\mathbf{k}}^2 \epsilon_{\gamma\mu\nu} v_\alpha(i, \mathbf{k}) v_\nu(i, \mathbf{k}) M_{\beta\mu}^{-1}(i, \mathbf{k}), \end{aligned} \quad (2)$$

where $\epsilon_{\gamma\mu\nu}$ is the Levi-Civita symbol, $\tau_{i,\mathbf{k}}$ is the relaxation time of the electron with the crystal momentum \mathbf{k} and the band index i , $v_\alpha(i, \mathbf{k})$ is its group velocity along the α direction, and $M_{\beta\mu}^{-1}(i, \mathbf{k})$ is its inverse effective mass tensor. In the present compound, the inverse effective mass tensor is almost diagonal with respect to the tetragonal axes; accordingly, the local Hall conductivity tensors are approximated as

$$\begin{aligned} \sigma_{xyz}(i, \mathbf{k}) &= -e^3 \tau_{i,\mathbf{k}}^2 v_x^2(i, \mathbf{k}) M_{yy}^{-1}(i, \mathbf{k}), \\ \sigma_{zxy}(i, \mathbf{k}) &= e^3 \tau_{i,\mathbf{k}}^2 v_z^2(i, \mathbf{k}) M_{xx}^{-1}(i, \mathbf{k}). \end{aligned} \quad (3)$$

The conductivity tensors can be obtained by integrating the local conductivity tensors multiplied by the derivative of the Fermi-Dirac distribution function ($-\partial f/\partial \epsilon$) over the entire Brillouin zone and summing over all band indices i . At low temperatures, $-\partial f/\partial \epsilon$ is approximated by the delta function; thus, the conductivity tensors in Eq. (1) are calculated from the surface integration of Eq. (3) on the Fermi surface. Since the Hall terms $\sigma_{\alpha\beta\gamma} B_\gamma$ and the off-diagonal terms $\sigma_{\alpha\beta}$ are sufficiently smaller than the diagonal terms $\sigma_{\alpha\beta}$, the Hall coefficients R_{ac} , R_{ab} are expressed as

$$R_{ab} = \frac{\sigma_{xyz}}{\sigma_{xx}^2}, \quad R_{ac} = \frac{-\sigma_{zxy}}{\sigma_{zz}\sigma_{xx}}. \quad (4)$$

To simplify the calculation, we assume that $\tau_{i,\mathbf{k}}$ is a constant with any i and \mathbf{k} ; thus, the Hall coefficient does not depend on τ . Seebeck coefficients S_a and S_c were also calculated from $\sigma_{\alpha\beta}$ and Fermi-Dirac distribution function [15].

R_{ac} , R_{ab} , and the anisotropy in the conductivity σ_{zz}/σ_{xx} thus calculated are plotted as a function of the number of electrons per Nb in Fig. 12(a). When the number of electrons per Nb is 0.20, which is the value for the stoichiometric compound, $|R_{ac}|$ is much smaller than $|R_{ab}|$, partly owing to the anisotropy in the conductivity $\sigma_{zz} \gg \sigma_{xx}$, but it does not agree with the experimental result. Anisotropy in the conductivity $\sigma_{zz}/\sigma_{xx} \sim 5$ is also not as large as the experimental value. However, with decreasing Fermi energy, the anisotropy in the conductivity is enhanced and the sign of R_{ab} is reversed from negative to positive. If we assume 0.08 electrons/Nb, corresponding to the Fermi energy of 0.15 eV lower than the value for the stoichiometric sample, R_{ac} is comparable to the experimental value of $\sim -4 \times 10^9 \text{ m}^3/\text{C}$, whereas R_{ab} is close to zero. Anisotropy in the conductivity $\sigma_{zz}/\sigma_{xx} \sim 14$ is also in a good agreement with the experimental value.

Seebeck coefficient also shows a good agreement with the experimental value of $\sim 50 \mu\text{V}/\text{K}$ both for $|S_a|$ and $|S_c|$ by

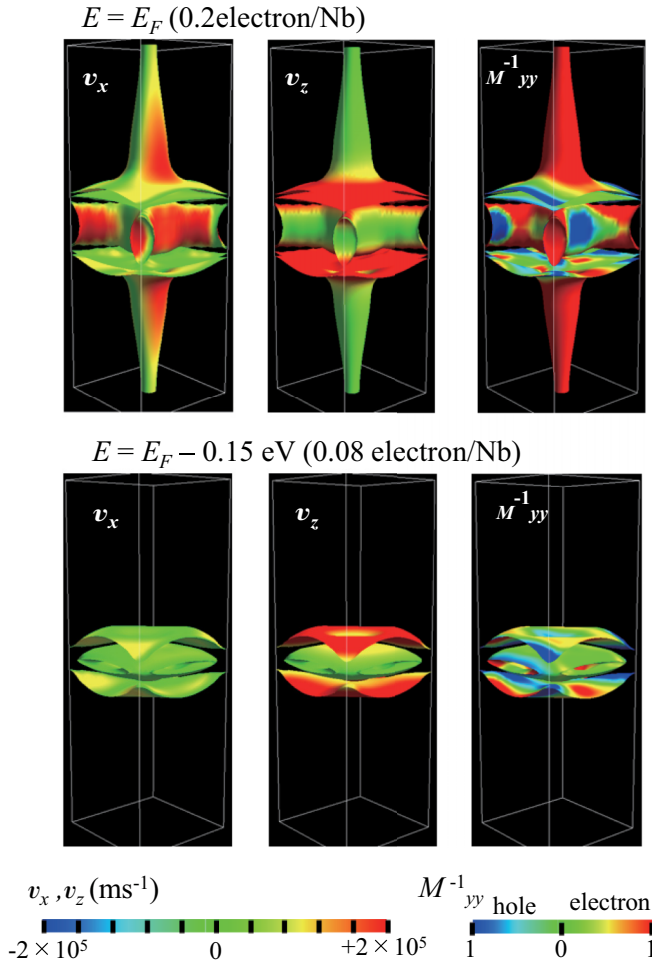


FIG. 11. Fermi velocities $v_x(i, \mathbf{k})$ and $v_z(i, \mathbf{k})$ and relative inverse effective mass tensor $M_{yy}^{-1}(i, \mathbf{k})$ at $E = E_F$ (upper panels) and $E = E_F - 0.15 \text{ eV}$ (lower panels).

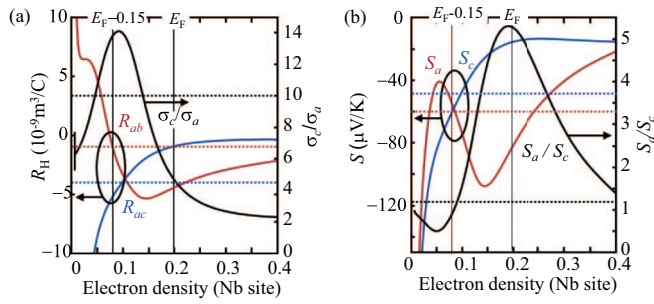


FIG. 12. (a) Calculated Hall coefficients R_{ab} and R_{ac} , the anisotropy in the conductivity σ_c/σ_a . (b) Seebeck coefficients S_a , S_c , and the anisotropy in the Seebeck coefficient S_a/S_b , as functions of the number of electrons per Nb site. In both panels, dotted horizontal lines correspond to the experimental values for $\text{Ba}_3\text{Nb}_5\text{O}_{15}$, and vertical solid lines correspond to the number of electrons per Nb for the stoichiometric (0.2) and slightly hole-doped (0.08, where E_F is lower by 0.15 eV) compositions.

assuming 0.08 electrons/Nb, although if 0.20 electrons/Nb is assumed, the calculated $|S_c|$ is too small whereas $|S_a|$ is too large compared with the experimental values, as shown in Fig. 12(b).

Experimentally, the number of d electrons per Nb estimated by TGA is 0.17, slightly lower than the stoichiometric value of 0.20, as described in the introduction, but is not as small as 0.08 suggested by the comparison with the band calculation. One possibility for this discrepancy is that not all the d electrons estimated by the chemical analysis become the itinerant electrons that contribute to the Fermi level, but some of them remain localized. Another possibility is that some branches of the band dispersion seen in Fig. 10 are pushed up in energy due to the electron correlation and thus, the band dispersion at the Fermi level of $n = 0.20$ in the real material becomes similar to that of $n = 0.08$ in the present band calculation.

The enhancement of the anisotropy in the conductivity with decreasing E_F can be explained by the disappearance of two-dimensional cylindrical Fermi surfaces but the existence of one-dimensional sheet-like Fermi surfaces, as shown in Fig. 11. The one-dimensional sheet-like Fermi surfaces have both the electron-like and hole-like curvatures along the xy plane. This can be seen in the lower panels of Fig. 11, where M_{yy}^{-1} is negative or positive depending on the direction of \mathbf{k} . On the other hand, the sheet-like Fermi surfaces have the electron-like curvature along the z direction, meaning that $M_{zz}^{-1} < 0$. This explains why $|R_{ac}|$ becomes larger than $|R_{ab}|$ as E_F decreases.

Finally, the T dependence of the magnetic susceptibilities when the magnetic field is applied along the c axis (χ_c) and the a axis (χ_a) are shown in Fig. 13. In this figure, the Larmor diamagnetism arising from the core electrons at each atom is subtracted from the data. As can be seen, the anisotropy of the magnetic susceptibility is negligible. χ for $x = 0$ is almost T independent, and this is most likely caused by the Pauli paramagnetism of the conduction electrons in the Nb $4d$ states. This T -independent behavior becomes T dependent; χ decreases with decreasing T for $x \geq 1.5$. This means that there is no local $4d$ moment, which should give a Curie-Weiss

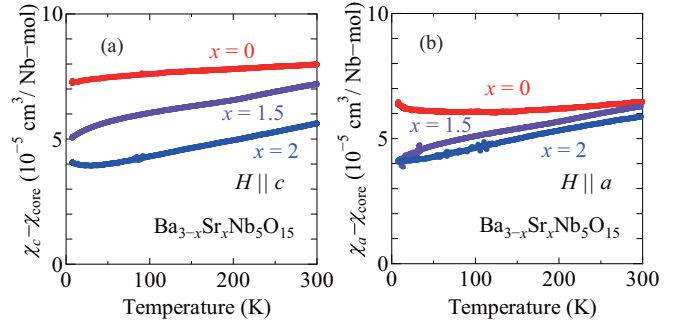


FIG. 13. Magnetic susceptibility of $\text{Ba}_{3-x}\text{Sr}_x\text{Nb}_5\text{O}_{15}$ along (a) the c axis and (b) the a axis.

behavior in $\chi(T)$ if it exists, in the Nb ions of this compound even in the insulating phase.

IV. DISCUSSION

Let us discuss the possible origin of the metal-insulator transition with x in $\text{Ba}_{3-x}\text{Sr}_x\text{Nb}_5\text{O}_{15}$. One possibility is a Mott transition. Even though the number of d electron per Nb is only 0.2, since there are ten Nb ions in one unit cell, it is possible that an integer number of d electrons exist at one cluster of Nb ions and become localized owing to the Coulomb repulsion. However, there are two experimental results that do not support this interpretation in this paper: (1) The magnetic susceptibility of usual Mott insulators exhibits a Curie-Weiss behavior arising from the magnetic moment of the localized electrons and thus, the phase transition from a metallic state to a Mott-insulating state should show a change in the magnetic susceptibility from a T -independent Pauli paramagnetic behavior to a Curie-Weiss behavior. This is the case for V_2O_3 [23,24] and perovskite titanates [25], typical compounds exhibiting Mott transitions. However, the magnetic susceptibility of the present compound does not show a Curie-Weiss behavior, as seen in Fig. 13. (2) In usual Mott transitions, the spectral weight of the Drude part in the optical conductivity spectrum $\sigma(\omega)$ is transferred to a Mott excitation dominated by the on-site Coulomb energy U in the insulating phase [26], but no such behavior was observed in the present series of compounds; the spectral weight of the Drude part simply decreases and $\sigma(\omega)$ at $\hbar\omega \sim 0$ decreases to zero with the metal-insulator transition (Fig. 6). This indicates that the on-site Coulomb energy is not as large as to dominate the metal-insulator transition in $\text{Ba}_{3-x}\text{Sr}_x\text{Nb}_5\text{O}_{15}$, although an important role of the Coulomb interaction in the present compounds was previously pointed out on the basis of hard x-ray photoemission spectroscopy results [7].

Another possibility is a phase transition into a band-insulating state. Since there is no change in the number of d electrons with x in this series of compounds, the only possibility is a transition from a semimetallic state to a band-insulating state, which arises from the shift of the conduction band and the valence band with x . However, this is inconsistent with some of the results in this paper: (1) The band calculation of $\text{Ba}_3\text{Nb}_5\text{O}_{15}$ indicates that all the Fermi surfaces are electron pockets but there is no hole pocket. (2) The behavior of the Hall coefficient barely changes with x up to $x = 1$,

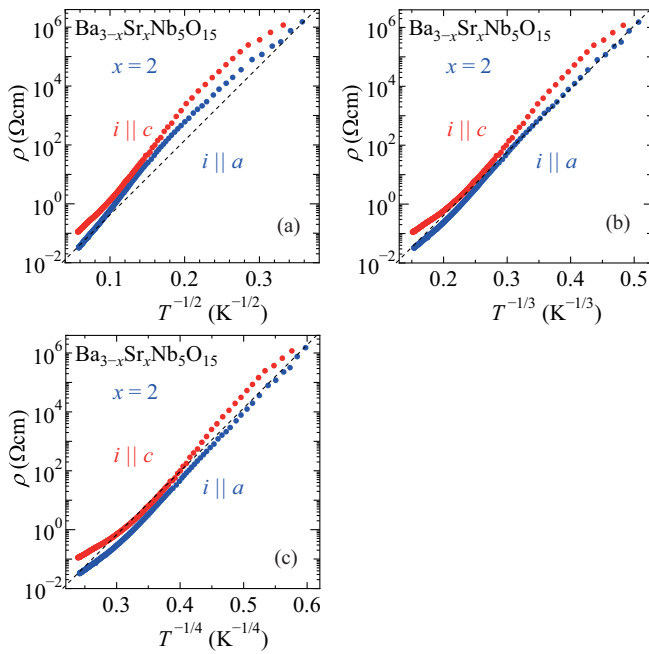


FIG. 14. The resistivity along the c axis (ρ_c) and the a axis (ρ_a) of $\text{Ba}_{3-x}\text{Sr}_x\text{Nb}_5\text{O}_{15}$ with $x = 2$ in a log scale as functions of (a) $T^{-1/2}$, (b) $T^{-1/3}$, and (c) $T^{-1/4}$. The dashed-straight line in each figure is guide to the eye.

although it is expected that both the number of electrons and that of holes decrease with increasing x in the semimetallic regime in this model.

One of the reasonable explanations for the metal-insulator transition is the insulating state caused by a disorder, as proposed in Ref. [6]. There are two inequivalent sites A1 and A2 with a 1:2 ratio for Ba of $\text{Ba}_3\text{Nb}_5\text{O}_{15}$ in the TTB structure, as shown in Fig. 1. Here, the Ba ion at the A1 site is tightly bound to 12 oxygen ions, similarly to the A site of the perovskite structure, whereas the surrounding of the A2 site is rather loose and there are only six Ba-O bonds shorter than 3 Å for the Ba ion at the A2 site (Fig. 1). Thus, the Sr ion, which is smaller than the Ba ion, will first be substituted for Ba at the A1 site up to $x = 1$ and then it will be substituted for Ba at the A2 site [5]. It is likely that the Sr ion at the A2 site is too small to be stably located at the symmetric position but randomly takes several positions with energy minima around the A2 site. This leads to a disorder in the crystal structure, resulting in the insulating behavior for $x > 1$. Note that this disorder exists even for the other end material $\text{Sr}_3\text{Nb}_5\text{O}_{15}$, since it is not substitutional disorder but the disorder arising from the Sr ions that are loosely bound to the neighboring ions. For this issue, to see if the T dependence of the resistivity for our single crystals is dominated by the variable-range-hopping (VRH) process, a typical transport process in the disordered system, the resistivity of $\text{Ba}_{3-x}\text{Sr}_x\text{Nb}_5\text{O}_{15}$ with $x = 2$ is plotted in a log scale as functions of $T^{-1/n}$ with $n = 2, 3$, and 4 in Fig. 14. As can be seen, $\log \rho_a$ becomes almost linear as a function of $T^{-1/3}$ ($n = 2$), suggesting two-dimensional VRH process, although ρ_c is slightly away from $T^{-1/n}$ for any of n . This result is consistent with that for the polycrystalline samples previously reported [6], which are mainly dominated by ρ_a .

The idea of the metal-insulator transition caused by disorder is consistent with various experimental results in this study. First, the absolute values of the resistivity barely change up to $x = 1$ but they increase (particularly at low T) for $x > 1$. The behavior of the Hall coefficient also barely changes up to $x = 1$. This can be explained by the fact that the substitution of Sr for Ba at the A1 site for $x < 1$ induces the least disorder, whereas the substitution for Ba at the A2 site for $x > 1$ induces a significant disorder. The anisotropy in the dc conductivity σ_c/σ_a decreases with increasing x experimentally, and this can be explained by the increase in the disorder of the Nb-O-Nb bond angle along the c axis, which is 180° without any disorder. The discrepancy between the anisotropy in the dc conductivity and that in the spectral weight of the optical conductivity below 1.4 eV can be explained by this model assuming that the distribution of the magnitude of the transfer integral Δt arising from the structural disorder is less than 1.4 eV. In such a case, even if the dc transport properties at $\hbar\omega = 0$ eV are severely affected by the disorder, the spectral weight up to 1.4 eV is less affected, resulting in the existence of anisotropy in the spectral weight even for $x = 2$. The behavior of magnetic susceptibility is also consistent with this model; there is no clear gap in the density of states but it is partially reduced in the insulating phase caused by the disorder, and this will induce a small suppression in the Pauli paramagnetic susceptibility, particularly at low T , with increasing x . Recent EXAFS measurement also confirms the model above. Namely, the Fourier transform of the EXAFS spectra for the Nb K-edge significantly changes with Sr doping for $3.5 - 4 \text{ \AA}$ [27], suggesting that the neighboring Nb-Nb bonds are locally modulated with Sr doping.

V. SUMMARY

In summary, we studied the single crystals of $\text{Ba}_{3-x}\text{Sr}_x\text{Nb}_5\text{O}_{15}$ ($0 \leq x \leq 2$) to clarify the origin of the metal-insulator transition and the anisotropy of the electronic structure. We found that the dc resistivity changes from being metallic ($d\rho/dT > 0$) to insulating ($d\rho/dT < 0$) across $x = 1.5$ both along the c axis (straight chains of Nb-O-Nb) ρ_c , and along the ab plane (zigzag chains of Nb-O-Nb) ρ_a , similarly to the polycrystalline samples. In particular, $\rho_c(T)$ barely changes with increasing x from 0 to 1 in the metallic phase. The anisotropy of dc conductivity (the inverse dc resistivity), $\sigma_c/\sigma_a = \rho_a/\rho_c$ is ~ 10 for $x = 0$, but with increasing x , it decreases and becomes close to unity in the insulating phase for $x \geq 1.5$. We also found that the optical conductivity $\sigma(\omega)$ derived from the optical reflectivity spectrum changes from a Drude-like spectrum to a spectrum with a peak at finite $\hbar\omega$ across $x = 1.5$, and the anisotropy of the spectral weight below $\hbar\omega = 1.4$ eV is ~ 2 in the metallic phase, but it persists, although slightly decreases, even in the insulating phase. The Hall coefficients R_{ac} (where the current is along the c axis and the voltage is along the a axis) are negative and their absolute values are larger than those of R_{ab} (where the current and voltage are both along the ab plane) for $x = 0$, and the behavior barely changes with increasing x up to $x = 1$. The Seebeck coefficients along the c and a axes are almost comparable for $x = 0$, which is in contrast to the behavior of the resistivity. The anisotropy of

the resistivity, the Hall coefficient, and the Seebeck coefficient can be quantitatively explained by band calculation with the number of electrons per Nb modified to 0.08. The magnetic susceptibility is almost T independent for $x = 0$, but slightly decreases with decreasing T for $x \geq 1.5$.

These experimental results indicate the one-dimensional characteristic of the electronic structure and transport properties in this series of compounds. The origin of the insulating state for $x \geq 1.5$ is most likely to be the disorder arising from

the Sr ions at the A2 site, which are bound to the surrounding oxygen ions quite loosely.

ACKNOWLEDGMENTS

We thank T. Mizokawa, T. Yasuda, and N. L. Saini for fruitful discussions. This work was supported by JSPS KAKENHI Grants No. 19H01853, No. 21H01038, and JST CREST Grant No. JPMJCR15Q2.

- [1] N. F. Mott, *Metal-Insulator Transitions* (Taylor & Francis, Philadelphia, 1974).
- [2] M. Imada, A. Fujimori, and Y. Tokura, Metal-insulator transitions, *Rev. Mod. Phys.* **70**, 1039 (1998).
- [3] B. Hessen, S. A. Sunshine, T. Siegrist, A. T. Fiory, and J. V. Waszczak, Structure and properties of reduced barium niobium oxide single crystals obtained from borate fluxes, *Chem. Mater.* **3**, 528 (1991).
- [4] B. Hessen, S. Sunshine, T. Siegrist, and R. Jimenez, Crystallization of reduced strontium and barium niobate perovskites from borate fluxes, *Mater. Res. Bull.* **26**, 85 (1991).
- [5] T. Kolodiazhnyi, H. Sakurai, O. Vasyukiv, H. Borodianska, and Y. Mozharivskiy, Abnormal thermal conductivity in tetragonal tungsten bronze $\text{Ba}_{6-x}\text{Sr}_x\text{Nb}_{10}\text{O}_{30}$, *Appl. Phys. Lett.* **104**, 111903 (2014).
- [6] T. Kolodiazhnyi, H. Sakurai, M. Isobe, Y. Matsushita, S. Forbes, Y. Mozharivskiy, T. J. S. Munsie, G. M. Luke, M. Gurak, and D. R. Clarke, Superconductivity and crystal structural origins of the metal-insulator transition in $\text{Ba}_{6-x}\text{Sr}_x\text{Nb}_{10}\text{O}_{30}$ tetragonal tungsten bronzes, *Phys. Rev. B* **92**, 214508 (2015).
- [7] T. Yasuda, Y. Kondo, T. Kajita, K. Murota, D. Ootsuki, Y. Takagi, A. Yasui, N. L. Saini, T. Katsufuji, and T. Mizokawa, Interplay between electronic correlation and atomic disorder in a low carrier density $4d$ transition-metal oxide, *Phys. Rev. B* **102**, 205133 (2020).
- [8] C. J. Raub, A. R. Sweedler, M. A. Jensen, S. Broadston, and B. T. Matthias, Superconductivity of Sodium Tungsten Bronzes, *Phys. Rev. Lett.* **13**, 746 (1964).
- [9] R. K. Stanley, R. C. Morris, and W. G. Moulton, Conduction properties of the hexagonal tungsten bronze, Rb_xWO_3 , *Phys. Rev. B* **20**, 1903 (1979).
- [10] N. Haldolaarachchige, Q. Gibson, J. Krizan, and R. J. Cava, Superconducting properties of the K_xWO_3 tetragonal tungsten bronze and the superconducting phase diagram of the tungsten bronze family, *Phys. Rev. B* **89**, 104520 (2014).
- [11] K. Ohgushi, A. Yamamoto, Y. Kiuchi, C. Ganguli, K. Matsubayashi, Y. Uwatoko, and H. Takagi, Superconducting Phase at 7.7 K in the Hg_xReO_3 Compound with a Hexagonal Bronze Structure, *Phys. Rev. Lett.* **106**, 017001 (2011).
- [12] L. D. Muhlestein and G. C. Danielson, Effects of ordering on the transport properties of sodium tungsten bronze, *Phys. Rev.* **158**, 825 (1967).
- [13] P. Giannozzi, S. Baroni, N. Bonini, M. Calandra, R. Car, C. Cavazzoni, D. Ceresoli, G. L. Chiarotti, M. Cococcioni, I. Dabo *et al.*, Quantum espresso: A modular and open-source software project for quantum simulations of materials, *J. Phys.: Condens. Matter* **21**, 395502 (2009).
- [14] M. Fuchs and M. Scheffler, Ab initio pseudopotentials for electronic structure calculations of poly-atomic systems using density-functional theory, *Comput. Phys. Commun.* **119**, 67 (1999).
- [15] G. K. Madsen and D. J. Singh, Boltztrap. A code for calculating band-structure dependent quantities, *Comput. Phys. Commun.* **175**, 67 (2006).
- [16] T. Osafune, N. Motoyama, H. Eisaki, and S. Uchida, Optical Study of the $\text{Sr}_{14-x}\text{Ca}_x\text{Cu}_{24}\text{O}_{41}$ System: Evidence for Hole-Doped Cu_2O_3 Ladders, *Phys. Rev. Lett.* **78**, 1980 (1997).
- [17] K. Takenaka, K. Nakada, A. Osuka, S. Horii, H. Ikuta, I. Hirabayashi, S. Sugai, and U. Mizutani, Anisotropic Optical Spectra of $\text{PrBa}_2\text{Cu}_4\text{O}_8$: Possible Tomonaga-Luttinger Liquid Response of the Quasi-One-Dimensional Metallic CuO Double Chains, *Phys. Rev. Lett.* **85**, 5428 (2000).
- [18] C. Presura, M. Popinciuc, P. H. M. van Loosdrecht, D. van der Marel, M. Mostovoy, T. Yamauchi, and Y. Ueda, Charge-Ordering Signatures in the Optical Properties of $\beta\text{-Na}_{0.33}\text{V}_2\text{O}_5$, *Phys. Rev. Lett.* **90**, 026402 (2003).
- [19] R. Murata, T. Sato, T. Okuda, Y. Horibe, H. Tsukasaki, S. Mori, N. Yamaguchi, K. Sugimoto, S. Kawaguchi, M. Takata, and T. Katsufuji, Electronic phase transition in hollandite titanates $\text{Ba}_x\text{Ti}_8\text{O}_{16+\delta}$, *Phys. Rev. B* **92**, 220408(R) (2015).
- [20] T. Okuda, K. Nakanishi, S. Miyasaka, and Y. Tokura, Large thermoelectric response of metallic perovskites: $\text{Sr}_{1-x}\text{La}_x\text{TiO}_3$ ($0 \leq x \leq 0.1$), *Phys. Rev. B* **63**, 113104 (2001).
- [21] T. Okuda, H. Hata, T. Eto, S. Sobaru, R. Oda, H. Kaji, K. Nishina, H. Kuwahara, M. Nakamura, and R. Kajimoto, Effects of Mn substitution on the thermoelectric properties and thermal excitations of the electron-doped perovskite $\text{Sr}_{1-x}\text{La}_x\text{TiO}_3$, *J. Phys. Soc. Jpn.* **85**, 094717 (2016).
- [22] A. Sakai, T. Kanno, S. Yotsushashi, A. Odagawa, and H. Adachi, Control of epitaxial growth orientation and anisotropic thermoelectric properties of misfit-type $\text{Ca}_3\text{Co}_4\text{O}_9$ thin film, *Jpn. J. Appl. Phys.* **44**, L966 (2005).
- [23] D. B. McWhan, A. Menth, J. P. Remeika, W. F. Brinkman, and T. M. Rice, Metal-insulator transitions in pure and doped V_2O_3 , *Phys. Rev. B* **7**, 1920 (1973).
- [24] S. A. Carter, T. F. Rosenbaum, J. M. Honig, and J. Spalek, New Phase Boundary in Highly Correlated, Barely Metallic V_2O_3 , *Phys. Rev. Lett.* **67**, 3440 (1991).
- [25] Y. Taguchi, Y. Tokura, T. Arima, and F. Inaba, Change of electronic structures with carrier doping in the highly correlated electron system $\text{Y}_{1-x}\text{Ca}_x\text{TiO}_3$, *Phys. Rev. B* **48**, 511 (1993).
- [26] T. Katsufuji, Y. Okimoto, and Y. Tokura, Spectral Weight Transfer of the Optical Conductivity in Doped Mott Insulators, *Phys. Rev. Lett.* **75**, 3497 (1995).
- [27] F. Stramaglia, N. L. Saini, T. Yasuda, T. Mizokawa, K. Katsufuji *et al.* (unpublished).